THE JOURNAL OF BIOLOGICAL CHEMISTRY VOL. 288, NO. 44, pp. 31830–31841, November 1, 2013

A Mutation in the Nuclear Pore Complex Gene *Tmem48* Causes Gametogenesis Defects in Skeletal Fusions with Sterility (*sks*) Mice*

Received for publication, June 7, 2013, and in revised form, September 2, 2013 Published, JBC Papers in Press, September 17, 2013, DOI 10.1074/jbc.M113.492306

Kouyou Akiyama[‡], Junko Noguchi[§], Michiko Hirose[¶], Shimpei Kajita[‖], Kentaro Katayama[‖1], Maryam Khalaj[‖2], Takehito Tsuji[‡], Heather Fairfield, Candice Byers**, Laura Reinholdt**, Atsuo Ogura[¶], and Tetsuo Kunieda[‡3]**

*From the [‡]Graduate School of Environmental and Life Science and [‖]Graduate School of Natural Science and Technology, Okayama University, 1-1-1, Tsushima-naka, Okayama 700-8530, Japan, the [§]Division of Animal Science, National Institute of Agrobiological Sciences, Tsukuba Ibaraki 905-8602, Japan, [¶]RIKEN Bioresource Center, Tsukuba, Ibaraki 305-0074, Japan, and **The Jackson Laboratory, Bar Harbor, Maine 04609*

Background: *sks* is a mouse mutant showing sterility caused by defects in meiosis.
Results: We found a mutation of the *Tmem48* gene encoding nuclear pore complex protein. The mutation causes aberrant splicing, resulting in deletion of an exon.
Conclusion: *Tmem48* is essential for meiosis and gametogenesis.
Significance: This is the first report to demonstrate that the nuclear pore complex has an important role in mammalian gametogenesis.

Skeletal fusions with sterility (*sks*) is an autosomal recessive mutation of mouse that results in male and female sterility because of defects in gametogenesis. The mutants also have skeletal malformations with fused vertebrae and ribs. We examined testicular phenotypes of *sks*/*sks* mice to investigate the defects in spermatogenesis. Histological and immunocytochemical analyses and expression analyses of the marker genes demonstrated that spermatogenesis is arrested at mid to late pachytene stage of meiotic prophase with defective synapsis of the homologous chromosomes. Next, we determined the precise chromosomal localization of the *sks* locus on a 0.3-Mb region of mouse chromosome 4 by linkage analysis. By sequencing the positional candidate genes in this region and whole exome sequencing, we found a GG to TT nucleotide substitution in exon 6 of the *Tmem48* gene that encodes a putative transmembrane protein with six transmembrane domains. The nucleotide substitution causes aberrant splicing, which deletes exon 6 of the *Tmem48* transcript. Specific expression of TMEM48 was observed in germ cells of males and females. Furthermore, the phenotypes of the *sks* mutant were completely rescued by the transgenesis of a genomic fragment containing the wild-type *Tmem48* gene. These findings indicate that the *Tmem48* mutation is responsible for the gametogenesis defects and skeletal malformations in the *sks* mice. The TMEM48 protein is a nuclear membrane protein comprising the nuclear pore complex; its exact function in the nuclear pore complex is still unknown. Our finding suggested that the nuclear pore complex plays an important role in mammalian gametogenesis and skeletal development.

Mammalian gametogenesis, particularly spermatogenesis, is a dramatic developmental process. It consists of cell proliferation, differentiation, and morphogenesis, which involve numerous cellular and molecular steps, including germ cell differentiation and germ cell/somatic cell interactions. In mouse, spermatogenesis begins 7 days after birth with the differentiation of gonocytes into spermatogonial stem cells and subsequent recruitment of differentiated spermatogonia into meiosis I with the formation of pre-leptotene primary spermatocytes. Meiosis I is characterized by a prolonged prophase, consisting of the leptotene, zygotene, pachytene, diplotene, and diakinesis stages, in which the pairing and recombination of homologous chromosomes are accompanied by changes in chromatin structure. Meiosis I is initiated by the formation of meiotic DNA double-strand breaks (DSBs)[4] at the leptotene stage, and these DSBs are repaired by homologous recombination in zygotene spermatocytes. During the zygotene and pachytene stages, homologous chromosomes undergo synapsis, a process mediated by the formation of the synaptonemal complex (SC), which plays an essential role in meiotic recombination (1). At the diplotene/diakinesis stages, the synaptonemal complexes disintegrate; following this, the condensed bivalent chromosomes align on the metaphase plate, and sister chromatids dissociate into two daughter cells.

To study the molecular mechanisms underlying mammalian gametogenesis, mutant mice with defective gametogenesis are useful animal models to identify the key molecules and signaling pathways (1, 2). So far, a large number of infertile and subinfertile animal models have been obtained by spontaneous mutations, gene targeting technology, and several mutagenesis

* This work was supported in part by Sasakawa Scientific Research Grant 18-130 from the Japan Science Society and grants from the Japan Society for the Promotion of Science.
[1] Present address: Nippon Veterinary and Life Science University, Tokyo 170-0071, Japan.
[2] Present address: NIDDK, National Institutes of Health, Bethesda, MD 20892.
[3] To whom correspondence should be addressed. Tel.: 81-86-251-8314; Fax: 81-86-251-8388; E-mail: tkunieda@cc.okayama-u.ac.jp.

[4] The abbreviations used are: DSB, DNA double-strand break; BAC, bacterial artificial chromosome; E*n*, embryonic day; ESE, splicing enhancer motif; NE, nuclear envelope; NPC, nuclear pore complex; P*n*, postnatal day; SC, synaptonemal complex; SNP, single-nucleotide polymorphism; SPB, spindle pole body; sqRT-PCR, semiquantitative RT-PCR; Tg, transgene.

TABLE 1
Nucleotide sequences of PCR primers

Primer	Forward	Reverse
H1t	CGGCCTCAAGTACCCTTGTTCC	TTTCTTGCCCTTGCCCTTGT
Hspa2	CAGACGCAGACCTTCACTAC	TTTTGTCCTGCTCGCTAATC
Ccna1	ATGAGTTTGTCTACATCACTGACG	GTTGGCCCCACTCTCAGAAACC
Sprm-1	GCTCCATTTTGATTTCCCCCACTA	CCCCAAGCTTCTGTAAACCACTCC
Hspl1	GGTGATGAGGGTCTGAAG	GGGTGGGGGTGTGAAAAG
Gapdhs	AACATCATCCCATCTTCCACT	TCCGTGATAGCCGAGTAAGAAG
Tnp1	AGCCGCAAGATAAAGACTCATGG	CACAAGTGGGATCGGTAATTGCG
Gapdh	CTTTGGCATTGTGGAAGGG	CCTCTCTTGCTGCAGTGTC
D4Mit331	CCTAACCCTCCCCACACC	AAAGATCTGGATTCAAATCCTCC
D4Mit168	GTTCCTCCAAACCCACCC	AAGAAAAGAAAATGAAAACGATGG
D4Mok20	CACAAAATACAGAACACTGACCCC	GAACACTGCTAACCAGAGGCTGT
D4Mit31	ACGAGTTGTCCTCTGATCAACA	AGCCAGAGCAAACACCAACT
D4Mok21	GAAGACAGGCTGGTTTCTCTGCAGA	CCTCAGAGCCTCCCCTGCGAA
D4Mok22	GTAGCACTCACATTACGGGAGGC	CATTTGGCCCCTGTGGCTACGAT
D4Mit43	TGTCTGTACTGTTCTGACTCTGTG	AGGAGAGAAGCCCTTATGCC
D4Mit146	AAAAATGACAGCATTATGTTGGG	CTCCCTCAGTCTTGCTTTGG
D4Mit199	CTACCATGGTCTCATAAATTGCC	TTAGATGGCAAGAGTAAGACAAACA
Tmem48-exon6_rtPCR	CCCTGCTGCTCAGACCTGCTT	CTGTGTGAAGGTCCAGAGCAGGTG
Tmem48-exon6_genome	GATGCTGAGTGTGTCCCTT	CAATGAAATCAGTTGGGCTGATC
pET01_cDNAlowen]primer	GATCCACGATGC	
pET01-exon A	CCAGGATCGATCCGCTTCCTG	
pET01-exon B	CCACCTCCAGTGCCAAGGTCTGAA	
Tmem48-exon 6	CTGACCATGAACAGGGATTCCACACA	
RP23-259O13-SP6	CCGTCGACATTTAGGTGACACTAT	CCCAGGACTCTCAGTGGTATCAA
RP23-259O13-T7	CACAAACCTGTCCTTAGTCTTGACA	GGATCCTCTCCCTATAGTGAGTCG
Glis1^{rs28129472}	CCAGTGGTTGTCTGATTCTGAAA	CAGGGGTTTGCATCAGAATATCTT
Yipf1^{rs28147349}	GGCAATTTGTTAAGAAGAGCTGGTA	CCCATTAACTTGCAGTGGATGTTGTT

projects; these animal models have certainly contributed to our understanding of the molecular mechanisms of mammalian gametogenesis (1–5). They are also valuable for gaining an understanding of the pathogenesis of human infertility, frequently due to defective gametogenesis. Skeletal fusions with sterility (*sks*) is an autosomal recessive mutation of mice that arose spontaneously in the A/J strain at The Jackson Laboratory. The *sks* mutant shows sterility and skeletal defects in both males and females, which are caused by defective gametogenesis and skeletal fusion, respectively (6). The *sks* mutant is, therefore, a good model to investigate the molecular mechanisms underlying both gametogenesis and axial skeleton development in mammals, and identifying the causative gene for the *sks* mutation will contribute to understanding the genes required for in these processes. Here, we report a detailed examination of defective spermatogenesis in *sks* mutants as well as the positional cloning and identification of the underlying mutation in *Tmem48*.

EXPERIMENTAL PROCEDURES

Mice and Histological Preparations—The *sks* mice that were used in this study were obtained from the Mouse Mutant Resource at The Jackson Laboratory. The JF1/Ms strain was obtained from the National Institute of Genetics (Mishima, Japan). The *sks* mutant and normal mice were euthanized, and tissues were excised and fixed by immersion in Bouin's fluid. After dehydration, tissues were embedded in paraffin wax and sectioned. After deparaffination in xylene, sections were rehydrated and stained with Mayer's hematoxylin and eosin. The protocols for the use of animals in this study were approved by the Animal Care and Use Committee of Okayama University.

Immunofluorescence Staining of Surface Spread Preparations of Testicular Cells—The surface spread preparations of testicular cells were prepared as described previously (7) with some modifications. Seminiferous tubules were dissociated in DMEM and centrifuged at 1800 rpm, and the collected cells were resuspended in DMEM. The cell suspension was spread onto the surface of the 0.5% NaCl solution, transferred to a silanized glass slide, and fixed with 2% paraformaldehyde containing 0.02% SDS. The surface-spread preparations were incubated with rabbit polyclonal anti-SCP3 antibody (8) that was diluted 1:500 and mouse monoclonal anti-γ-H2AX (JBW301; Upstate, Lake Placid, NY) that was diluted 1:300, and the preparations were incubated with rhodamine-conjugated donkey anti-rabbit IgG (AP182R, Chemicon International) that was diluted 1:200 and goat anti-mouse IgG-Alexa Fluor 488 (A-21121; Invitrogen) that was diluted 1:400 as secondary antibodies.

Semiquantitative (sq) RT-PCR Analysis—Total RNA samples of adult tissues, whole embryos of E10.5, testes of juvenile mice at various ages, ovaries of pubertal mice (21 days old), and each stage of the estrous cycle of adult mice were subjected to sqRT-PCR analyses. Total RNA from mouse tissues was extracted using TRIzol (Invitrogen) according to the manufacturer's instructions. RNA preparations were treated with 10 units of DNase I (TaKaRa Bio, Shiga, Japan) and then purified. cDNA synthesis was performed by a reverse transcription reaction using Superscript III reverse transcriptase (Invitrogen) and oligo(dT) primer (Invitrogen) according to the manufacturer's instructions. The amounts of RNA were standardized according to the amplification of an internal control using the murine GAPDH primers (Table 1). The expression of stage-specific marker genes was examined by RT-PCR analysis by using primers that are listed in Table 1 as described in Dix *et al.* (9). sqRT-PCR was also performed to evaluate the expression pattern of the *Tmem48* gene using primer pairs that are listed in Table 1. RT-PCR analysis was carried out in a reaction mixture containing a 100 nM concentration of each primer, a 100 μM concentration of each dNTP, and 0.25 unit of *Taq* polymerase (TaKaRa

Bio) with 25–30 cycles of amplification that consisted of 94 °C for denaturation, 53 °C-60 °C for annealing, and 72 °C for extension. The PCR products were electrophoresed on agarose gels.

Linkage Mapping and Positional Cloning of the sks Gene—To determine the chromosomal location of the *sks* locus, we performed linkage analysis using 532 F_2 mice obtained by intercross of F_1 mice derived from a cross between the *sks* and JF1/Ms mouse strains. To map the *sks* locus, genotypes of microsatellite makers of the F_2 mice were determined by PCR in a reaction mixture containing 20 ng of genomic DNA, a 100 nM concentration of each primer for the microsatellite markers (Table 1), a 100 μM concentration of each dNTP, and 0.25 unit of *Taq* polymerase (TaKaRa Bio) with 35 cycles of amplification that consisted of 94 °C for denaturation, 53 °C-60 °C for annealing, and 72 °C for extension.

For sequence analyses of the positional candidate genes, entire coding regions of the candidate genes were amplified by sets of primers (Table 1), cloned in the pGEM T-easy vector (Promega), and sequenced by the dideoxy chain termination method with a DNA sequencer HITACHI SQ5500.

For whole exome sequencing, size selected DNA (Pippen Prep; Sage Science) and Illumina Paired End libraries were constructed from genomic DNA using the Illumina-supplied protocol. Hybridization-based sequence capture was used to enrich the Illumina library for all mouse coding sequences (exome). Roche NimbleGen SeqCap EZ Mouse Exome Design (110624_MM9_Exome L2R_D02_EZ_HX1) was utilized according to the manufacturer's protocols and as described by Fairfield *et al.* (10). After capture, enriched sequencing libraries used for cluster formation and paired end sequencing were done using Illumina HiSeq. Sequencing data were processed and aligned to the mouse genome (MGSC37, mm9) using a Burrows-Wheeler Alignmer, and SNPs/INDELs were called using SAMtools.

In Vitro Splicing Assay—The exon-trapping vector (Exontrap, pET01; MoBiTec, Göttingen, Germany) was used to investigate the splicing activity of exon 6 of the *Tmem48* gene with the *sks* mutation. A 286-bp DNA fragment containing exon 6 and its flanking regions of the *Tmem48* gene of the *sks* or wild-type allele was cloned into the pET01 vector. The clone carrying DNA from either wild-type (pET01-+) or *sks* alleles (pET01-*sks*) was transiently expressed in COS7 cells. COS7 cells were cultured in DMEM with 10% FCS and were seeded 24 h before transfection. COS7 cells were transfected with 1 μg of pET01-+ or pET01-*sks* using FuGENE 6 (Roche Diagnostics). Total RNA was extracted from COS7 cells 48 h after transfection, cDNA was synthesized with a primer for pET01–3′ transcriptional region, and RT-PCR was carried out using 2 sets of primers, pET01-exonA and pET01-exonB, or *Tmem48*-exon 6-specific primer and pET01-exonB (Table 1).

Transgenesis Rescue of the sks Phenotypes—A BAC clone, RP23-259O13 (Invitrogen), containing an ~181-kb genomic fragment covering the *Tmem48* gene that was cloned into the pBACe3.6 vector, was used for BAC transgenesis rescue experiments (see Fig. 8*A*). A DNA fragment containing the 181-kb BAC insert and flanking vector sequences was used for the pronuclear injection to generate the BAC transgenic mice containing the wild-type *Tmem48* gene (see Fig. 8*A*). To genotype the transgenic animals, two sets of primers were used that amplified a 251-bp fragment of the T7 side of the pBACe3.6 vector-insert junction and a 289-bp fragment of the SP6 side of the pBACe3.6 vector-insert junction (see Fig. 8*B* and Table 1).

Immunohistochemical Analysis Using Anti-TMEM48 Antibody—A synthetic oligopeptide (HQKRLQQFLEFKE) that was derived from the C-terminal region of the mouse TMEM48 protein was used to immunize rabbits, and antibodies were purified from the serum of these rabbits. The specificity of the antibody was evaluated as follow. The Tmem48 protein fused with an N-terminal FLAG tag was expressed in COS7 cells by transfecting Tmem48/pCMV-Tg2. Lysates of transfected COS7 cells were electrophoresed through SDS-PAGE and transferred to a membrane, and the membrane was incubated with anti-TMEM48 or anti-FLAG M2 monoclonal antibody and goat anti-rabbit IgG HRP or goat anti-mouse IgG HRP as a secondary antibody. A neutralization test was also performed to test the antibody specificity. The antibody was preincubated with 0.5 mg/ml TMEM48 antigen before immunohistochemical staining. For immunofluorescence analysis of the transfected COS7 cells with anti-TMEM48 or anti-FLAG antibody, donkey anti-rabbit IgG rhodamine-conjugated (AP182R; Chemicon) and goat anti-mouse IgG-Alexa Fluor 488 (A-21121; Invitrogen) were used as secondary antibodies.

For the immunohistochemical analysis, tissue sections were incubated with PBS containing 0.3% H_2O_2 for 30 min and TNB buffer (0.1 M Tris-HCl, pH 7.5, 0.15 M NaCl, 0.5% tyramide signal amplification blocking reagent) for 30 min at room temperature. The sections were then incubated with the rabbit anti-TMEM48 antibody (1:500) with 3% BSA in PBS overnight at 4 °C. The sections were incubated in series with HRP-conjugated anti-rabbit IgG (sc-2004, B0507; Santa Cruz Biotechnology) diluted with 3% BSA in PBS (1:1000), 2,4-dinitrophenylhydrazine (DNP) amplification reagents, anti-DNP-HRP antibody (PerkinElmer Life Sciences), and 3,3′-diaminobenzidinetetrahydrochloride chromogen (Dako, Kyoto, Japan). The sections were counterstained with Mayer's hematoxylin and were examined by light microscopy.

Western Blot Analysis—Mouse testes were lysed in the radioimmunepreciptation assay buffer (150 mM NaCl, 10 mM Tris-HCl, pH 7.2, 0.1% SDS, 1% Triton X-100, 1% sodium deoxycholate, 5 mM EDTA, and 1 mM protease/phosphatase inhibitors). Equal amounts of the extracted proteins of the *sks*/*sks* and +/+ mice were separated by 7.5% SDS-PAGE and transferred to an Immobilon-P membrane (Millipore). The filters were incubated with anti-TMEM48 antibody that was diluted in 2% blocking buffer. The filters were washed with PBS-Tween 20 and then were incubated with HRP-conjugated goat anti-rabbit IgG. The HRP signal was detected using the Amersham Biosciences ECL Advance Western blotting Detection Kit (GE Healthcare) according to the manufacturer's instructions.

RESULTS

Spermatogenesis in sks Mice Is Interrupted at the Pachytene Stage of Meiotic Prophase—The testes of adult *sks*/*sks* mice were smaller than those of normal littermate animals, but the

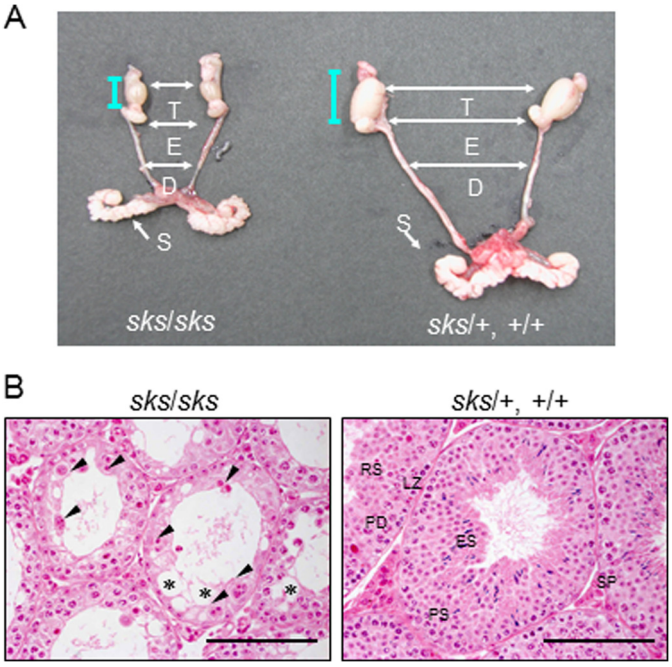

FIGURE 1. **Male gonads of *sks* and normal mice.** *A*, external appearances of testis (*T*), epididymis (*E*), spermatic duct (*D*), and seminal vesicle (*S*). *B*, hematoxylin and eosin-stained testis sections of adult mutant (*sks*/*sks*) and normal mice. The stages of the seminiferous tubule are classified according to Russell *et al.* (12). *SP*, intermediate spermatogonia; *LZ*, leptotene/zygotene spermatocytes; *PS*, pachytene spermatocytes; *PD*, pachytene/diplotene spermatocytes; *RS*, round spermatids; and *ES*, elongated spermatids. *Arrows* indicate vacuolar structures, and *arrowheads* indicate multinucleated cells. *Scale bars*, 100 μm.

sizes of other male reproductive organs, including the epididymis and seminal vesicle, showed no clear difference (Fig. 1*A*). The testis weights of adult *sks*/*sks* mice (0.045 $\pm$ 0.004 g) were less than one-fourth of those of normal mice (0.206 $\pm$ 0.046 g). Histological examination of the testes showed that most seminiferous tubules of the *sks*/*sks* mice contained germ cells at all stages of development up to pachytene stage, but neither spermatids nor spermatozoa were observed, and significant portions of seminiferous tubules were vacuolized (Fig. 1*B*) as reported previously (6). To further investigate the underlying spermatogenesis defect in the mutant mouse, we compared testis sections of *sks*/*sks* mice and normal littermates during the first wave of spermatogenesis at postnatal day (P) 14, 16, 18, 22, and 35 (Fig. 2) when spermatogenesis is synchronized (11). The seminiferous tubules of the mutant and normal mice showed an organized progression of cell types from spermatogonia at the periphery to leptotene, zygotene, or early-mid pachytene stage spermatocytes at the innermost layers at P14, and no significant difference was observed in the two genotypes (Fig. 2, *A* and *B*). At P16, mid-late pachytene spermatocytes and a few meiotic metaphase cells were apparent in the seminiferous tubules of the normal mice (Fig. 2*C*), and spermatocytes completed meiosis at P18 with the appearance of the round spermatids (Fig. 2*E*). However, although a few mid-late pachytene spermatocytes were observed, neither metaphase cells nor round spermatids were observed in the testes of the mutant mice at these stages (Fig. 2, *D* and *F*). More substantial differences appeared at later stages. The seminiferous tubules of the normal mice were filled with round spermatids at P22 (Fig. 2*G*) and showed

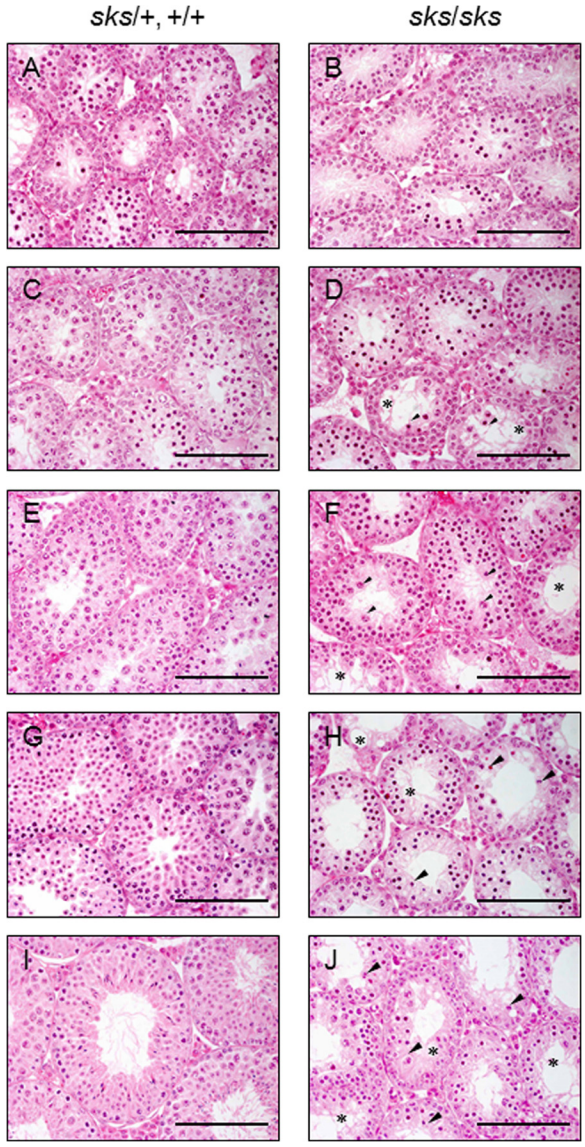

FIGURE 2. **First wave of spermatogenesis of the *sks* and normal mice.** Hematoxylin and eosin-stained testis sections of P14 (*A* and *B*), P16 (*C* and *D*), P18 (*E* and *F*), P22 (*G* and *H*), and P35 (*I* and *J*) from normal (*sks*/+ or +/+) (*A*, *C*, *E*, *G*, and *I*) and *sks*/*sks* (*B*, *D*, *F*, *H*, and *J*) mice. *Arrows* indicate meiotic metaphases, and *arrowheads* indicate multinucleated cells. *Arrowheads* indicate vacuolar structures. *Scale bars*, 100 μm.

the release of mature spermatozoa into the lumen at P35 (Fig. 2*I*), but the seminiferous tubules of the mutant mice contained no postmeiotic germ cells, and cells with condensed nuclei and multinucleated cells were frequently observed (Fig. 2, *H* and *J*). These findings indicate that the differentiation of most mutant germ cells is interrupted at mid to late pachytene stage of meiosis, although a few meiotic metaphase cells were observed in the seminiferous tubules of the adult mutant mice (Fig. 1*B*).

Expression of Stage-specific Marker Genes of Spermatogenesis—We examined the expression of the genes that have a stage-specific expression pattern during spermatogenesis by sqRT-PCR analysis to determine when the germ cell development was interrupted in the *sks*/*sks* mice. RT-PCR analysis of adult testis of the mutant mice revealed normal expression of the *Histh1t* gene, significantly reduced *Hspa2* and *Ccna1* gene expression, and no or trace levels *Pou5f2*, *Hspl1*, and *Tnp1* gene expression

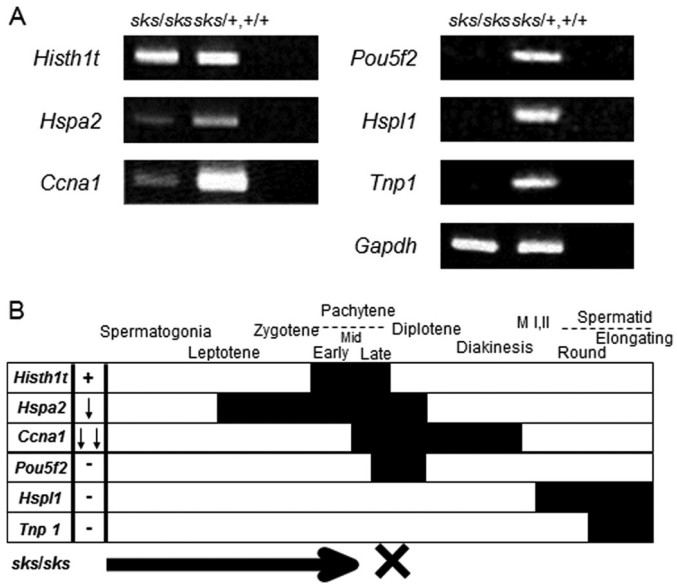

FIGURE 3. **Expression of the stage-specific marker genes in spermatogenesis of *sks*/*sks* and normal mice.** *A*, sqRT-PCR of testis RNA isolated from *sks*/*sks* and normal (*sks*/+ or +/+) mice. The amounts of RNA were normalized according to the expression level of the *Gapdh* gene. The *right lanes* are negative controls without cDNA. *B*, schematic representation of the expression stages of the marker genes during spermatogenesis showing the stage of arrest of spermatogenesis in the *sks*/*sks* mice.

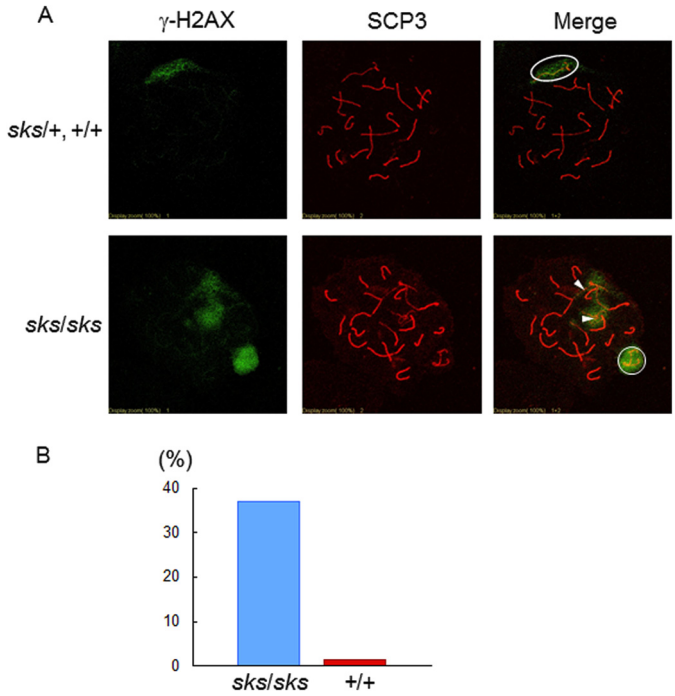

FIGURE 4. **Abnormal synapsis of homologous chromosomes in spermatocytes of *sks* mice.** *A*, localization of γH2AX signals in pachytene spermatocytes of *sks*/*sks* and normal (*sks*/+ or +/+) mice. *Circles* indicate γH2AX foci of the XY body that represents unpaired regions of the X and Y chromosomes in pachytene spermatocytes. *Arrowheads* indicate γH2AX foci of unpaired autosomes that were observed in pachytene spermatocytes of *sks*/*sks* mice. *Red*, SCP3 representing the synaptonemal complex. *Green*, γ-H2AX. *B*, frequency of synapsis failures in the pachytene spermatocytes of the *sks*/*sks* and normal mice.

(Fig. 3). The expression of genes that are specifically expressed at stages later than late pachytene stage in normal mice was not detected in the *sks*/*sks* mice. These results confirmed that spermatogenesis of the *sks*/*sks* mice is arrested at the late pachytene stage.

Surface Spread Preparation of Spermatocytes—During prophase of meiosis, a homologous chromosomes pair and a SC is formed between the homologous chromosomes. We examined whether pairing of homologous chromosomes and the formation of SC proceeded normally in the *sks*/*sks* spermatocytes by immunofluorescence staining using antibodies against SCP3 and γH2AX. SCP3 is a component of the lateral element of SC, and γH2AX is a phosphorylated histone variant that accumulates on the DSB sites and can be used as a maker for asynapsis. The patterns of γH2AX staining in the *sks*/*sks* spermatocytes at the leptotene to zygotene stage were similar to those of the normal mice. (data not shown). However, ~40% of the mutant spermatocytes at the pachytene stage showed apparently different γH2AX staining patterns. As shown in Fig. 4, a γH2AX focus was restricted to the X-Y body in the normal spermatocytes, which represented an unpaired region of the X and Y chromosomes. However, defused γH2AX foci other than the X-Y body were frequently observed in the *sks*/*sks* spermatocytes which indicates unrepaired DSBs in autosomes. These spermatocytes with the defused γH2AX foci also showed partial asynapsis of homologous chromosomes that was indicated by SCP3 signals (Fig. 4, *A* and *B*). These findings confirmed defects of homologous chromosome paring and synapsis in the spermatocytes of the *sks*/*sks* mice as reported previously (6).

Linkage Mapping of the sks Locus—We performed fine mapping of the *sks* locus by linkage analysis to identify the gene responsible for the *sks* mutation. A total of 532 F_2 progeny were obtained from the cross between *sks* and JF1/Ms mice. As the *sks* locus has been mapped to a 8-Mb interval of the distal region of mouse chromosome 4, we genotyped 9 microsatellite makers in this region in the 63 *sks*/*sks* and 469 unaffected mice. The segregation data of these makers indicated the localization of the *sks* gene to an ~0.3-Mb interval between *D4Mit31* and *D4Mok22* in which nine genes were localized (Fig. 5).

Characterization of the Candidate Genes in the sks Locus—We sequenced the entire coding regions of these nine genes: *Tceanc2*, *Tmem59*, *Ldlrad1*, *Lrrc42*, *Hspb11*, *Dio1*, *Yipf1*, *Tmem48*, and *Gils1*. Comparing the nucleotide sequences of these candidate genes in the *sks* mutant and normal mice revealed no nucleotide sequence differences in these genes except for the *Tmem48* gene. However, a remarkable difference was observed in the transcripts of the *Tmem48* gene. As shown in Fig. 6*A*, the amplification of cDNA spanning exon 6 of the gene by RT-PCR yielded a fragment with the expected size (287 bp) in the normal mouse, but the fragment from the mutant mouse was ~100 bp shorter than the expected size. Comparing the nucleotide sequence of these two transcripts revealed that a 109-bp sequence corresponding to exon 6 of the *Tmem48* gene was deleted in the transcripts of the mutant mice. RT-PCR analysis of *Tmem48* in several tissues showed that the deletion of exon 6 of *Tmem48* transcripts was observed in all of the *sks*/*sks* tissues but not the normal tissues, indicating that the deletion of exon 6 is not caused by tissue-specific alternative splicing. The deletion of exon 6 creates a frameshift mutation resulting in premature termination at codon 225. By Western blot analysis using anti-TMEM48 antibody, we confirmed that

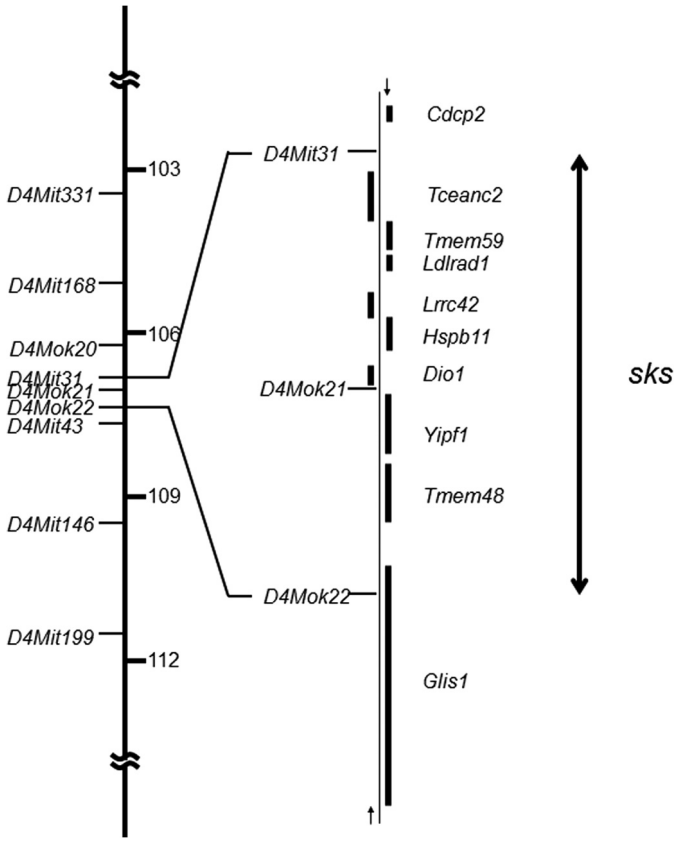

FIGURE 5. **Localization of the *sks* locus on mouse chromosome 4.** *Left*, map of the *sks* critical region in relationship to linked microsatellite markers; *right*, physical map corresponding to the *sks* critical region with positional candidate genes. The *vertical arrow* indicates the 0.3-Mb critical region.

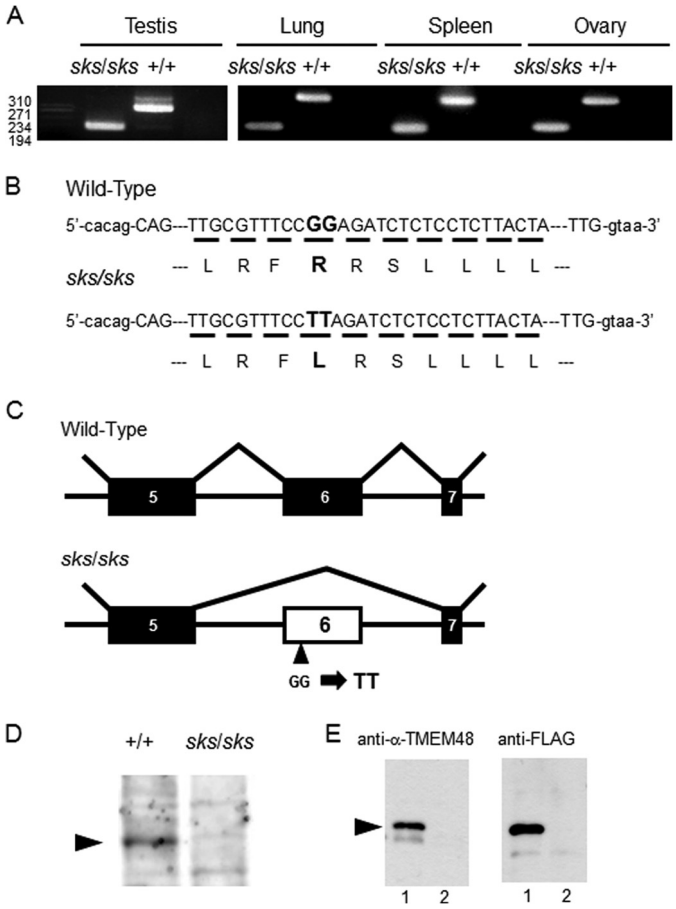

FIGURE 6. **Aberrant splicing and nucleotide substitution of the *Tmem48* gene in the *sks* mutant allele.** *A*, RT-PCR of mutant and wild-type *Tmem48* transcripts that were amplified from lung, spleen, and ovary RNAs. *B*, nucleotide sequences of the *sks* mutant and wild-type alleles showing a nucleotide substitution of GG to TT in the *sks* allele that resulted in an amino acid substitution of arginine (*R*) to leucine (*L*). *C*, splicing pattern of the *Tmem48* gene in the *sks* mutant and wild-type alleles. *D*, Western blot analysis of testis extracts using anti-TMEM48 antibody indicating the absence of TMEM48 protein in the *sks* mutant. The *arrowhead* indicates a specific band of TMEM48 with a molecular mass of 65 kDa. *E*, Western blotting of FLAG-tagged Tmem48 showing specificity of the antibody. Anti-TMEM48 antibody showed a specific band with a molecular mass of 65 kDa in the lysates of COS7 cells transfected with Tmem48/pCMV-Tg2. The same band was also detected by the anti-FLAG antibody. *Lanes 1*, COS7 with Tmem48/pCMV-Tg2. *Lanes 2*, intact COS7 without vector.

no mature TMEM48 protein was present in the tissues of *sks*/*sks* mice, whereas a protein of 65 kDa was observed in the normal mice (Fig. 6*D*). To determine the cause of the deletion, we compared the genomic sequence of *Tmem48* in the *sks* mutant and normal mice. Neither deletion of the region containing exon 6 nor mutation at the splicing donor or acceptor sites of the exon was observed, but a nucleotide substitution of GG to TT was found in exon 6 (Fig. 6*B*). Although the GG to TT substitution is predicted to result in a missense mutation of arginine to leucine, it also occurs in a putative exonic splicing enhancer motif (ESE), which likely explains the aberrant splicing observed in *sks* mice (Fig. 6*C*).

To confirm that the GG to TT substitution of *Tmem48* gene is unique to *sks* mice and no other gene of the candidate region has nucleotide lesion in the *sks* mice, we performed whole exome sequencing of *sks* mouse. Using the data generated from high throughput sequencing of whole exomes, we performed a genome-wide comparison of coding sequence from *sks* and from a strain background matched control (A/J). This comparison allowed us to eliminate from consideration all strain background-specific SNPs. We also compared these data with a large set (250) of whole exome datasets from unrelated spontaneous mutants and control inbred strains generated by the Jackson Laboratory Mutant Mouse Resource. As result, we confirmed that the GG to TT nucleotide substitution at 4:107053225–107053226 (MGSC37, mm9) in exon 6 of *Tmem48* was unique to *sks* and not found in any other strains of mice. We also confirmed the absence of any other lesion in the remaining genes in the candidate region including *Tceanc2*, *Tmem59*, *Ldlrad1*, *Lrrc42*, *Hspb11*, *Dio1*, *Yipf1*, and *Gils1*. These findings strongly suggested that the GG to TT substitution is the cause of the deletion of exon 6 in *Tmem48* gene of *sks* mice.

In Vitro Assay for the Splicing of the Mutant sks Gene—To confirm the relation between the nucleotide substitution in exon 6 and the deletion of exon 6 in the *sks* mouse, we examined the effect of the nucleotide substitution on the splicing of the gene by an *in vitro* splicing assay using the pET01-*sks* and pET01-+ vector containing the mutant and wild-type exon 6 and a part of introns 5 and 6 into pET01, respectively (Fig. 7*A*). COS7 cells were transfected by these vectors, and the splicing pattern of transcripts of the transfected COS7 cells was analyzed by RT-PCR. As shown in Fig. 7*B*, whereas the pET01-+ produced a significant amount of transcripts containing exon 6,

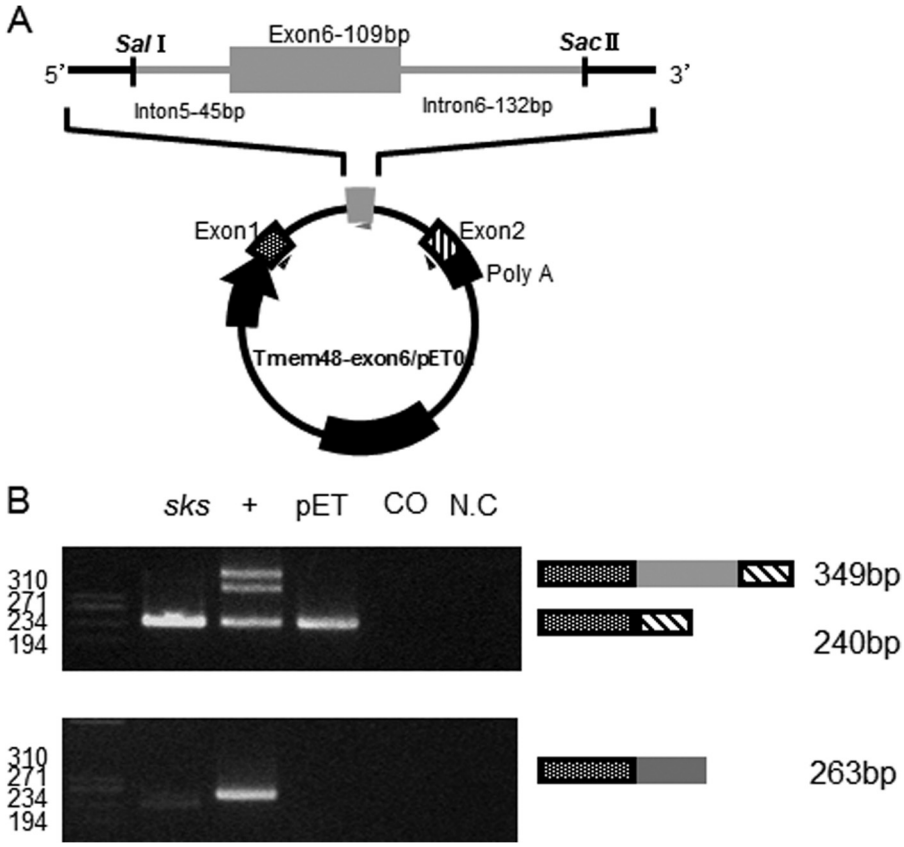

FIGURE 7. **Effects of the GG to TT nucleotide substitution of *Tmem48* on splicing.** *A*, construct of the exon-trapping vector pET01 for the *in vitro* splicing assay. *Arrowheads* indicate the location of primers that were used for RT-PCR. *B*, RT-PCR products showing splicing patterns of transcripts obtained from COS7 cells that were transfected with pET01 vectors. *sks*, cells that were transfected with pET01 with the *sks* exon 6 of *Tmem48*. +, cells that were transfected with pET01 with the wild-type exon 6 of *Tmem48*. *pET*, cells that were transfected with pET01 with no insert. *CO*, untransfected cells. *NC*, negative control without cDNA. The *dotted*, *gray*, and *striped boxes* indicate pET01-exonA, *Tmem48*-exon 6, and pET01-exon B, respectively.

no transcripts containing exon 6 were produced from pET01-*sks*. These findings demonstrated that that the GG to TT nucleotide substitution of the *Tmem48* gene is responsible for the deletion of exon 6 that was caused by the aberrant splicing.

Transgenesis Rescued the sks Phenotypes—To confirm that the nucleotide substitution of the *Tmem48* gene is responsible for the phenotypes of the *sks*/*sks* mice, we generated transgenic mice with a wild-type *Tmem48* transgene. The transgenic mice were generated by pronuclear injection of the genomic fragment obtained from a BAC clone containing the wild-type *Tmem48* gene. As shown in Fig. 8*A*, the 181-kb BAC RP23 insert indicated as the *gray bar* contains entire exons, introns, and the promoter region of the *Tmem48* gene, but it contains only a 3′ and 5′ part of the flanking genes, *Yipf1* and *Glis1*, respectively. Therefore, the functional gene in this BAC fragment is only the *Tmem48* gene. The resultant *Tmeme48* transgene-positive (Tg^+) transgenic mice were crossed with *sks*/+ mice, and the *sks*/*sks*;Tg^+ mice were obtained by a cross between the *sks*/+;Tg^+ and *sks*/+ mice. All resultant *sks*/*sks*;Tg^+ mice are viable and morphologically indistinguishable from their normal littermates, and the no skeletal abnormality was observed (Fig. 8, *C* and *E*). Both males and females showed normal fertility, and no abnormality in the spermatogenesis was observed by histological examination (Fig. 8*D*). Therefore, the wild-type *Tmem48* gene completely rescued the phenotypes of the *sks*/*sks* mice, demonstrating that the nucleotide substitution of *Tmem48* is responsible for the phenotypes of the *sks* mice.

Expression Analysis of the Tmem48 Gene—Expression analysis by sqRT-PCR of various tissues of wild-type mice revealed that the *Tmem48* gene was expressed in several mouse tissues, including testis, ovary, and E10.5 embryos (Fig. 9*A*). Subsequently, *Tmem48* expression in testes of P2 to P32 juvenile mice during the first wave of spermatogenesis was examined to determine whether the *Tmem48* gene is expressed at the specific stages of spermatogenesis. As a result, *Tmem48* expression was detected in all developmental stages of testes (Fig. 9*B*), indicating no stage-specific expression of *Tmem48* in differentiating germ cells. We also examined *Tmem48* expression in ovaries of juvenile mice (3 weeks old) and different stages of the estrous cycle of adult mice; we found expression in the ovaries of juvenile and adult mice, and the expression levels changed depending on the stages: the highest expression level was detected in the diestrus stage, and the lowest level was detected in the metestrus stage (Fig. 9*C*).

Immunohistochemical Analysis—The localization of the TMEM48 protein in the testes of the wild-type mice was examined by immunohistochemistry using anti-TMEM48 antibody. The results revealed the stage-specific localization of TMEM48 in testicular germ cells. As shown in Fig. 10, we classified the stages of the cycle of the seminiferous epithelium according to Russell *et al.* (12). Positive immunological reactivity for

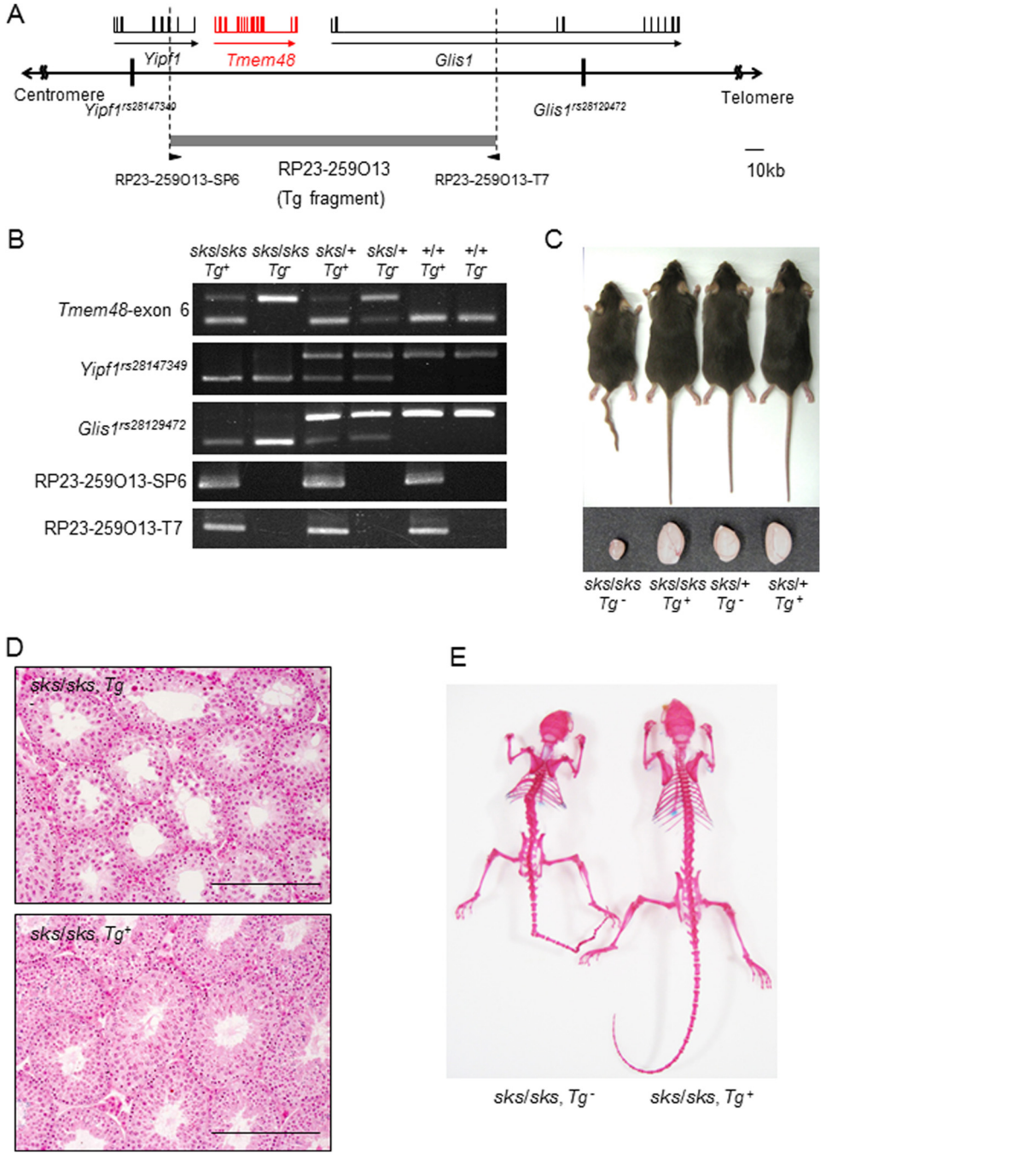

FIGURE 8. **Rescue of *sks* phenotypes by transgenic mice with wild-type *Tmem48* gene.** *A*, physical map of the genomic region including the *Tmem48* gene. The positions of the *Tmem48* gene and the flanking *Yipf1* and *Glis1* genes are indicated. SNPs *Yipf1*^{rs} and *Glis1*^{rs} were used to distinguish the endogenous and transgenic *Tmem48* genes. *B*, genotyping of the endogenous and transgenic *Tmem48* genes of transgenic mice that were crossed with *sks* mice. The *upper* and *lower bands* of *Tmem48*-exon 6 represent the *sks* and wild-type *Tmem48* allele, respectively. The *upper* and *lower bands* of *Yipf1*^{rs} and *Glis1*^{rs} SNPs are associated with the *sks* and wild-type allele, respectively. RP23-SP6 and RP23T7 are PCR fragments represent SP6 and T7 sides of the pBACe3.6-insert junctions, respectively. *C*, gross appearance of the transgenic *sks* mice, showing rescue of *sks* phenotypes including small body size, kinky tail, and small testis in *sks*/*sks*;*Tg*$^{+}$. *D*, histology of testes of the transgenic *sks* mice showing normal spermatogenesis in *sks*/*sks*;*Tmem48*$^{TG/+}$. *Scale bars*, 100 μm.

TMEM48 was observed in the cytoplasm of round and elongating spermatids in the stage I seminiferous epithelium, round spermatids in stages II–VI, and round or elongating spermatids and pachytene or diplotene spermatocytes in stages VII–XI (Fig. 10*A*). In stage XII, immunological reactivity was observed in elongating spermatids but not in the spermatocytes in metaphase (Fig. 10*A*). In contrast, no immunological reactivity was observed in other types of testicular germ cells, including spermatogonia, leptotene, and zygotene spermatocytes, elongated spermatids, and somatic cells like Leydig and Sertoli cells (Fig. 10*A*). Although the localization of TMEM48 on the nuclear envelope is not clear in the immunohistochemical staining of the testis sections, clear localization of TMEM48 on the nuclear envelope was observed in cultured COS7 cells that were transfected with the *Tmem48* gene (Fig. 10*D*). These results indicate that TMEM48 was specifically expressed in the cytoplasm and

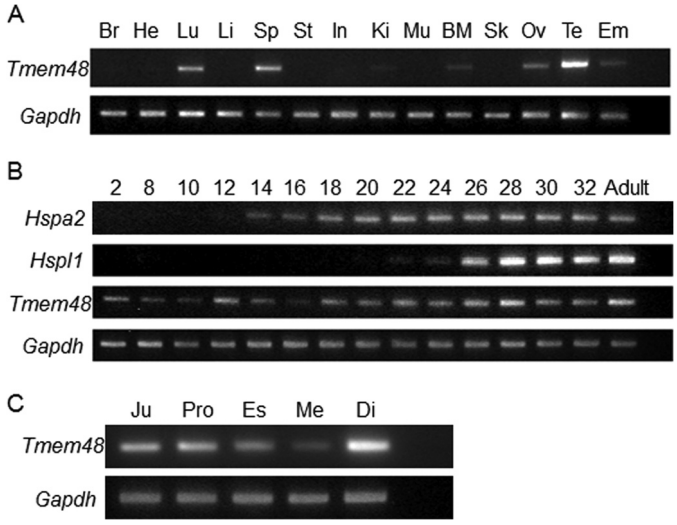

FIGURE 9. **Expression of the *Tmem48* gene in mouse tissues and developmental stages.** *A*, expression of the *Tmem48* gene in mouse brain (*Br*), heart (*He*), lung (*Lu*), liver (*Li*), spleen (*Sp*), Stomach (*St*), intestine (*In*), kidney (*Ki*), skeletal muscle (*Mu*), bone marrow (*BM*), skin (*Sk*), ovary (*Ov*), and testis (*Te*) of adult mouse, and whole embryos (*Em*) at E10.5. *B*, expression of the *Tmem48* gene in mouse testis during the first wave of spermatogenesis. The expression patterns of *Hspa2*, which is expressed after spermatocytes reach the zygotene stage, and *Hspl1*, which is expressed after the round spermatid stage, are indicated for comparison. *C*, expression of the *Tmem48* transcripts in ovary at different stages of the estrous cycle. *Ju*, juvenile (3 weeks after birth); *Pro*, proestrus; *Es*, estrus; *Me*, metestrus; and *Di*, diestrus. The amounts of RNA were normalized according to the expression level of the *Gapdh* gene.

the nuclear envelope during mid pachytene spermatocytes to step 13 elongating spermatids of spermatogenesis except for the spermatocytes in metaphase, in which the nuclear envelope disappears. Furthermore, strong cytoplasmic staining of TMEM48 protein was also observed in the oocytes of wild-type ovaries (data not shown). These results showing TMEM48 expression in germ cells of specific developmental stages suggested a specific function for TMEM48 in mouse gametogenesis.

DISCUSSION

In this study, we identified a nucleotide substitution of GG to TT in exon 6 of *Tmem48* that is accompanied by defective splicing that excludes exon 6 in the *Tmem48* transcripts of *sks* mutant mice. We also demonstrated that the GG to TT substitution is sufficient to cause skipping of exon 6 in an *in vitro* splicing assay. These findings indicate that the nucleotide substitution in exon 6 is responsible for the deletion of exon 6 in the transcripts. Various nucleotide substitutions have been reported to cause human genetic defects with splicing abnormalities (13). Most of these nucleotide substitutions directly affected canonical splicing signals, including the 5′ splicing donor, branching, and/or 3′ splicing acceptor sites. Nucleotide substitutions that create an ectopic splice site have also been reported (13). However, nucleotide substitutions in the coding region of genes generally affect the function of the genes by changing the amino acid sequences. The nucleotide substitution of the *sks* mutant also was predicted to cause an amino acid substitution of arginine to leucine in a highly conserved region of the protein. Besides the possible amino acid substitution, however, some nucleotide substitutions in exons are known to impair normal splicing, and genetic defects caused by aberrant splicing via nucleotide substitutions in exons have also been reported (13, 14). For example, a G to A missense mutation in exon 5 of the *PMM2* gene, which is associated with carbohydrate-deficient glycoprotein syndrome type Ia, causes a deletion of exon 5 in the transcripts of the gene (15). In these exon-skipping mutations, the nucleotide substitutions disrupt putative ESEs. ESEs are *cis*-acting elements that stimulate splicing (13) and are thought to serve as binding sites for a family of splicing factors such as SF2/ASF, SC35, SRp40, and SRp50 (13). Therefore, the nucleotide substitution of the *sks* mouse was suggested to disrupt ESEs in exon 6 of the *Tmem48* gene.

ESEs have consensus motifs, and software that identifies putative ESEs and evaluates whether exonic mutations disrupt the ESEs has been developed. We examined whether the nucleotide substitution of the *Tmem48* gene disrupts ESEs in exon 6 using these programs. ESEfinder 3.0 (16) can search for sequences that act as binding sites for four splicing enhancer proteins. ESEfinder predicted that the nucleotide substitution of GG to TT disrupted SF2/ASF and SRp40 binding motifs of exon 6. We also evaluated the effect of the nucleotide substitution using Rescue-ESE v1.0, which predicts the ESEs based on a list of hexamer motifs that are enriched in exons (17). Rescue-ESE predicted that two ESEs that are found in exon 6 of wild-type *Tmem48* are missing in the *sks* mutant. These results strongly suggested that the exon skipping of the *Tmem48* gene is caused by disrupted ESEs in exon 6 of the *Tmem48* gene by the GG to TT nucleotide substitution.

The *Tmem48* gene comprises 18 exons and encodes a transmembrane protein of 673 amino acids with six transmembrane domains. *Tmem48* is homolog of *NDC1*, a nuclear pore complex (NPC) protein of *Saccharomyces cerevisiae* (18, 19). The Ndc1 protein serves as a membrane-anchored protein to connect the NPC to the nuclear envelope (NE) (20, 21). Recently, the human NDC1 protein was also reported to be essential for NPC assembly and NE formation (20, 21). The NPC is a large protein complex that crosses the NE and is composed of approximately 30 nucleoporin proteins (22). NDC1 is known to interact with the nucleoporin NUP53, which is tightly associated with the nuclear membrane and physically interacts with other NPC proteins, including NUP155 (20, 23). In the *Drosophila* mutant of the *Nup155* homologous gene, spermatogenesis arrested at prophase of meiosis I, the transition to metaphase did not occur, and oogenesis failed to progress into the vitellogenic stage; this resulted in sterility in both sexes (24). Furthermore, Thomas and Botstein have reported that the budding yeast *NDC1* mutant could not produce normal asci, which was caused by the failure of chromosome separation at meiosis (18). In this study, we found that the spermatogenesis of *sks* mice arrested at prophase of meiosis I, and TMEM48 protein expression was observed in spermatocytes at pachytene and diplotene stages of meiotic prophase. Furthermore, the *sks* mice showed defects in the synapsis of homologous chromosomes during meiotic prophase. These phenotypic similarities between of the *sks* mouse and the fruit fly and yeast with mutations in *NPC* genes suggested that the NPC has specific functions for meiosis, particularly in chromosome synapsis and separation. The major function of the NPC is thought to be the transport of water-soluble molecules across the NE, which

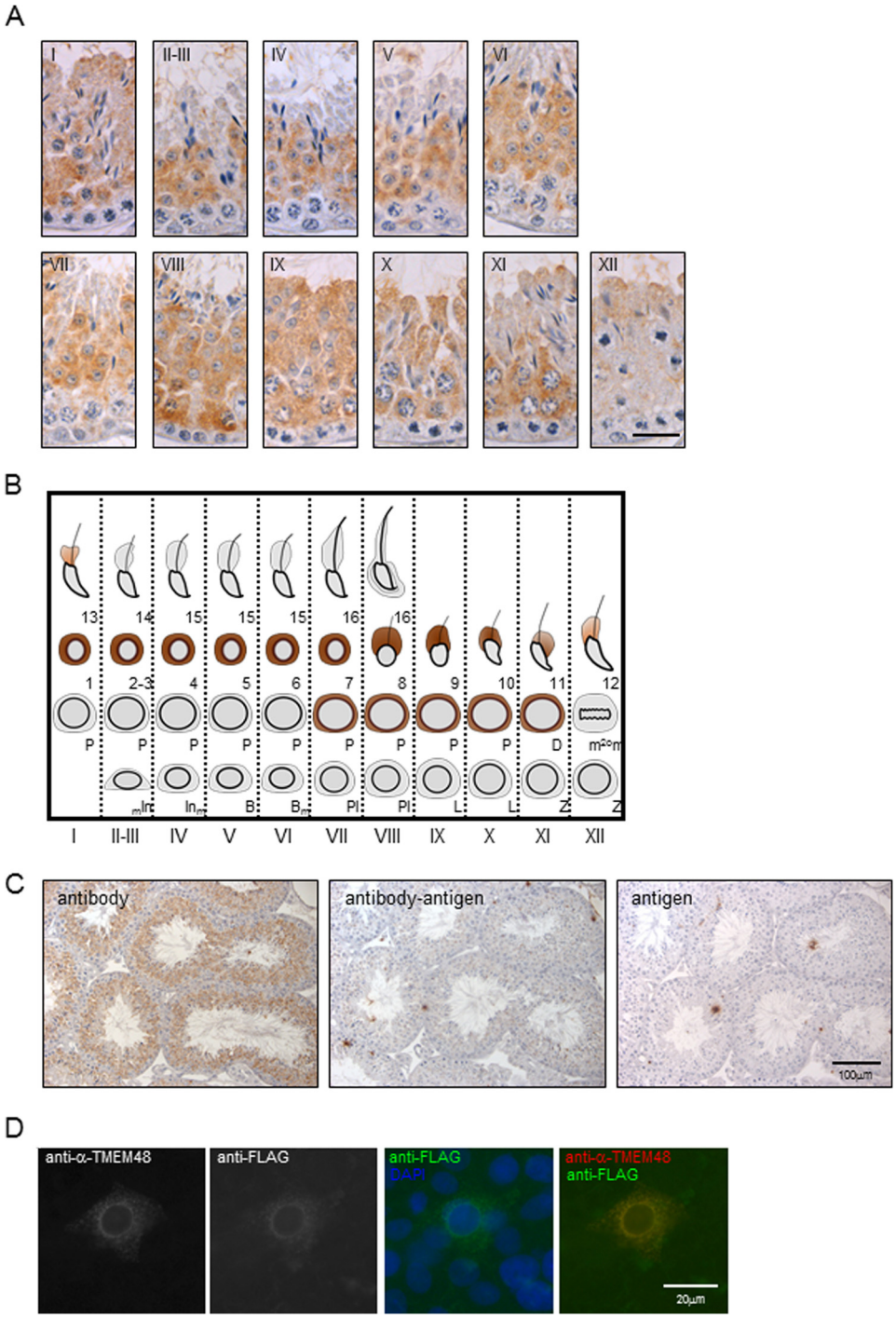

FIGURE 10. **Localization of TMEM48 in mouse seminiferous epithelium.** *A*, immunohistochemical staining of mouse testis using anti-TMEM48 antibody and counterstaining with hematoxylin. *I–XII* represent the stage of the cycle of the seminiferous epithelium. Positive signals with 3,3′-diaminobenzidinetetrahydrochloride staining were observed as *brown color*. *Scale bars*, 100 μm. *B*, schematic representation of the cycle of the seminiferous epithelium according to Russell *et al.* (12). $_{m}In$, intermediate spermatogonia; In_{m}, intermediate spermatogonia; *B*, type B spermatogonia; *Pl*, preleptotene spermatocyte; *L*, leptotene spermatocyte; *Z*, zygotene spermatocyte; *P*, pachytene spermatocyte, $m^{2o}m$, metaphase spermatocyte; *1–16*, steps 1–16 for spermatids. The localization of TMEM48 is indicated by *brown color*. *C*, neutralization test showing the specificity of the anti-TMEM48 antibody. The positive signals for the anti-Tmem48 antibody in testicular section disappeared when the antibody was preincubated with Tmem48 antigen before immunohistochemical staining. *D*, immunofluorescence analysis of the Tmem48/pCMV-Tg2-transfected COS7 cells with anti-TMEM48 or anti-FLAG antibody. Foci of anti-TMEM48 antibody and anti-FLAG antibody were colocalized on nuclear envelope of the transfected COS7 cells. *Red* and *green* signals indicate anti-TMEM48 antibody and anti-FLAG antibody, respectively. Counterstaining was done with DAPI.

includes the export of RNA molecules from the nucleus to the cytoplasm and the import of particular nuclear proteins into the nucleus (25). The function of NPC in meiosis and gametogenesis is unclear, but the nuclear import of certain proteins, including those comprising chromatin and the synaptonemal complex, is required for the progression of meiosis. Therefore, the mutation of *Tmem48* in *sks* mice might affect the transport of particular molecules that are essential

for the synapsis of homologous chromosomes during meiosis through the NPC.

The *S. cerevisiae* Ndc1 and the *Schizosaccharomyces pombe* homolog of the NDC1 protein localize not only to the nuclear pore but also the spindle pole body (SPB) and is known to be essential for the formation of SPBs (18, 26). The SPB is the microtubule-organizing center in yeast cells and is functionally equivalent to the centrosome in higher eukaryotes (27, 28). Several lines of genetic and cytological evidence suggest that SPBs or microtubules interact with the telomeres of chromosomes during prophase of meiosis I because all telomeres transiently gather at the NE and cluster around the SPB in fission yeast or the centrosome in mammals (29). This polarized chromosome arrangement is called the meiotic telomere clustering or the bouquet formation (29, 30). The bouquet formation coincides with the leptotene-zygotene transition stage, in which the pairing of homologous chromosomes begins (31). Therefore, the function of the bouquet formation in meiosis is predicted to ensure the efficient initiation of the synapsis of homologous chromosomes. Whether the Ndc1 protein is actually necessary for the bouquet formation and the lack of the *NDC1* gene causes the failure of the bouquet formation are not clear, but the localization of Ndc1 in the SPB suggests a possible role of Ndc1 in the bouquet formation. Therefore, the arrest of meiosis with defective synapsis that was observed in the *sks* mice could be caused by defective bouquet formation during meiosis.

Although the molecular mechanisms controlling mammalian gametogenesis are not fully understood because of its complexity, this is the first report to demonstrate that an NPC protein is essential for the proper progression of meiosis during mammalian gametogenesis. Additionally, *sks* mice, which show defects in gametogenesis that are caused by a mutation in the *Tmem48* gene, will be a useful model for studying the function of the NPC in meiosis and gametogenesis.

Acknowledgments—We thank Drs. N. Nakatsuji and S. Chuma for providing the antibody against SCP3.

REFERENCES

1. Handel, M. A., and Schimenti, J. C. (2010) Genetics of mammalian meiosis: regulation, dynamics and impact on fertility. *Nat. Rev. Genet.* **11,** 124–136
2. Matzuk, M. M., and Lamb, D. J. (2002) Genetic dissection of mammalian fertility pathways. *Nat. Cell Biol.* **4,** S41–49
3. Akiyama, K., Akimaru, S., Asano, Y., Khalaj, M., Kiyosu, C., Masoudi, A. A., Takahashi, S., Katayama, K., Tsuji, T., Noguchi, J., and Kunieda, T. (2008) A new ENU-induced mutant mouse with defective spermatogenesis caused by a nonsense mutation of the syntaxin 2/epimorphin (*Stx2*/*Epim*) gene. *J. Reprod. Dev.* **54,** 122–128
4. La Salle, S., Palmer, K., O'Brien, M., Schimenti, J. C., Eppig, J., and Handel, M. A. (2012) *Spata22*, a novel vertebrate-specific gene, is required for meiotic progress in mouse germ cells. *Biol. Reprod.* **86,** 45
5. Sun, F., Palmer, K., and Handel, M. A. (2010) Mutation of *Eif4g3*, encoding a eukaryotic translation initiation factor, causes male infertility and meiotic arrest of mouse spermatocytes. *Development* **137,** 1699–1707
6. Handel, M. A., Lane, P. W., Schroeder, A. C., and Davisson, M. T. (1988) New mutation causing sterility in the mouse. *Gamete Res.* **21,** 409–423
7. Noguchi, J., Ozawa, M., Nakai, M., Somfai, T., Kikuchi, K., Kaneko, H., and Kunieda, T. (2008) Affected homologous chromosome pairing and phosphorylation of testis specific histone, H2AX, in male meiosis under FKBP6 deficiency. *J. Reprod. Dev.* **54,** 203–207
8. Chuma, S., and Nakatsuji, N. (2001) Autonomous transition into meiosis of mouse fetal germ cells *in vitro* and its inhibition by gp130-mediated signaling. *Dev. Biol.* **229,** 468–479
9. Dix, D. J., Allen, J. W., Collins, B. W., Poorman-Allen, P., Mori, C., Blizard, D. R., Brown, P. R., Goulding, E. H., Strong, B. D., and Eddy, E. M. (1997) HSP70–2 is required for desynapsis of synaptonemal complexes during meiotic prophase in juvenile and adult mouse spermatocytes. *Development* **124,** 4595–4603
10. Fairfield, H., Gilbert, G. J., Barter, M., Corrigan, R. R., Curtain, M., Ding, Y., D'Ascenzo, M., Gerhardt, D. J., He, C., Huang, W., Richmond, T., Rowe, L., Probst, F. J., Bergstrom, D. E., Murray, S. A., Bult, C., Richardson, J., Kile, B. T., Gut, I., Hager, J., Sigurdsson, S., Mauceli, E., Di Palma, F., Lindblad-Toh, K., Cunningham, M. L., Cox, T. C., Justice, M. J., Spector, M. S., Lowe, S. W., Albert, T. Donahue, L. R., Jeddeloh, J., Shendure, J., and Reinholdt, L. G. (2011) Mutation discovery in mice by whole exome sequencing. *Genome Biol.* **12,** R86
11. Bellvé, A. R., Cavicchia, J. C., Millette, C. F., O'Brien, D. A., Bhatnagar, Y. M., and Dym, M. (1977) Spermatogenic cells of the prepubertal mouse: isolation and morphological characterization. *J. Cell Biol.* **74,** 68–85
12. Russell, L. D., Ettlin, R. A., Sinha Hihim, A. P., and Clegg, E. D. (1990) *Histological and Histopathological Evaluation of the Testis*, Cache River Press, Clearwater, FL
13. Cartegni, L., Chew, S. L., and Krainer, A. R. (2002) Listening to silence and understanding nonsense: exonic mutations that affect splicing. *Nat. Rev. Genet.* **3,** 285–298
14. Blencowe, B. J. (2000) Exonic splicing enhancers: mechanism of action, diversity and role in human genetic diseases. *Trends Biochem. Sci.* **25,** 106–110
15. Vuillaumier-Barrot, S., Barnier, A., Cuer, M., Durand, G., Grandchamp, B., and Seta, N. (1999) Characterization of the 415G>A (E139K) PMM2 mutation in carbohydrate-deficient glycoprotein syndrome type Ia disrupting a splicing enhancer resulting in exon 5 skipping. *Hum. Mutat.* **14,** 543–544
16. Cartegni, L., Wang, J., Zhu, Z., Zhang, M. Q., and Krainer, A. R. (2003) ESEfinder: a web resource to identify exonic splicing enhancers. *Nucleic Acids Res.* **31,** 3568–3571
17. Fairbrother, W. G., Yeo, G. W., Yeh, R., Goldstein, P., Mawson, M., Sharp, P. A., and Burge, C. B. (2004) RESCUE-ESE identifies candidate exonic splicing enhancers in vertebrate exons. *Nucleic Acids Res.* **32,** W187–190
18. Thomas, J. H., and Botstein, D. (1986) A gene required for the separation of chromosomes on the spindle apparatus in yeast. *Cell* **44,** 65–76
19. Winey, M., Hoyt, M. A., Chan, C., Goetsch, L., Botstein, D., and Byers, B. (1993) NDC1: a nuclear periphery component required for yeast spindle pole body duplication. *J. Cell Biol.* **122,** 743–751
20. Mansfeld, J., Güttinger, S., Hawryluk-Gara, L. A., Panté, N., Mall, M., Galy, V., Haselmann, U., Mühlhäusser, P., Wozniak, R. W., Mattaj, I. W., Kutay, U., and Antonin, W. (2006) The conserved transmembrane nucleoporin NDC1 is required for nuclear pore complex assembly in vertebrate cells. *Mol. Cell* **22,** 93–103
21. Stavru, F., Hülsmann, B. B., Spang, A., Hartmann, E., Cordes, V. C., and Görlich, D. (2006) NDC1: a crucial membrane-integral nucleoporin of metazoan nuclear pore complexes. *J. Cell Biol.* **173,** 509–519
22. Chatel, G., and Fahrenkrog, B. (2011) Nucleoporins: leaving the nuclear pore complex for a successful mitosis. *Cell. Signal.* **23,** 1555–1562
23. Hawryluk-Gara, L. A., Shibuya, E. K., and Wozniak, R. W. (2005) Vertebrate Nup53 interacts with the nuclear lamina and is required for the assembly of a Nup93-containing complex. *Mol. Biol. Cell* **16,** 2382–2394
24. Gigliotti, S., Callaini, G., Andone, S., Riparbelli, M. G., Pernas-Alonso, R., Hoffmann, G., Graziani, F., and Malva, C. (1998) *Nup154*, a new *Drosophila* gene essential for male and female gametogenesis, is related to the *Nup155* vertebrate nucleoporin gene. *J. Cell Biol.* **142,** 1195–1207
25. Strambio-De-Castillia, C., Niepel, M., and Rout, M. P. (2010) The nuclear pore complex: bridging nuclear transport and gene regulation. *Nat. Rev. Mol. Cell Biol.* **11,** 490–501
26. West, R. R., Vaisberg, E. V., Ding, R., Nurse, P., and McIntosh, J. R. (1998) *cut11*$^{+}$: a gene required for cell cycle-dependent spindle pole body anchoring in the nuclear envelope and biopolar spindle formation in *Schizosaccharomyces pombe*. *Mol. Biol. Cell* **9,** 2839–2855

27. Byers, B., Shriver, K., and Goetsch, L. (1978) The role of spindle pole bodies and modified microtubule ends in the initiation of microtubule assembly in *Saccharomyces cerevisiae*. *J. Cell Sci.* **30,** 331–352
28. Hyams, J. S., and Borisy, G. G. (1978) Nucleation of microtubules *in vitro* by isolated spindle pole bodies of the yeast *Saccharomyces cerevisiae*. *J. Cell Biol.* **78,** 401–414
29. Harper, L., Golubovskaya, I., and Cande, W. Z. (2004) A bouquet of chromosomes. *J. Cell Sci.* **117,** 4025–4032
30. Scherthan, H. (2001) A bouquet makes ends meet. *Nat. Rev. Mol. Cell Biol.* **2,** 621–627
31. Zickler, D., and Kleckner, N. (1998) The leptotene-zygotene transition of meiosis. *Annu. Rev. Genet.* **32,** 619–697